

Reliable magnetic reversible assembly of complex microfluidic devices: fabrication, characterization, and biological validation

Marco Rasponi · Francesco Piraino ·
Nasser Sadr · Matteo Laganà ·
Alberto Redaelli · Matteo Moretti

Received: 1 September 2010 / Accepted: 15 November 2010 / Published online: 30 November 2010
© Springer-Verlag 2010

Abstract Current standard procedures for fabrication of microfluidic devices combine polydimethylsiloxane (PDMS) replica molding with subsequent plasma treatment to obtain an irreversible sealing onto a glass/silicon substrate. However, irreversible sealing introduces several limitations to applications and internal accessibility of such devices as well as to the choice of materials for fabrication. In the present work, we describe and characterize a reliable, flexible and cost effective approach to fabricate devices that reversibly adhere to a substrate by taking advantage of magnetic forces. This is shown by implementing a PDMS/iron micropowder layer aligned onto a microfluidic layer and coupled with a histology glass slide,

in union with either temporary or continuous use of a permanent magnet. To better represent the complexity of microfluidic devices, a Y-shaped configuration including lower scale parallel channels on each branch has been employed as reference geometry. To correctly evaluate our system, current sealing methods have been reproduced on the reference geometry. Sealing experiments (pressure control, flow control and hydraulic characterization) have been carried out, showing consistent increases in terms of maximum achievable flow rates and pressures, as compared to devices obtained with other available reversible techniques. Moreover, no differences were detected between cells cultured on our magnetic devices as compared to cells cultured on permanently sealed devices. Disassembly of our devices for analyses allowed to stain cells by hematoxylin and eosin and for F-actin, following traditional histological processes and protocols. In conclusion, we present a method allowing reversible sealing of microfluidic devices characterized by compatibility with: (i) complex fluidic layer configurations, (ii) micrometer sized channels, and (iii) optical transparency in the channel regions for flow visualization and inspection.

Francesco Piraino and Nasser Sadr have contributed equally.

M. Rasponi (✉) · F. Piraino · A. Redaelli
Bioengineering Department, Politecnico Di Milano, Piazza
Leonardo Da Vinci 32, 20133 Milan, Italy
e-mail: marco.rasponi@polimi.it

F. Piraino
e-mail: francesco.piraino@polimi.it

A. Redaelli
e-mail: alberto.redaelli@polimi.it

N. Sadr · M. Moretti
IRCCS Istituto Ortopedico Galeazzi, Via Galeazzi 4, 20161
Milan, Italy
e-mail: nasser.sadr@polimi.it

M. Moretti
e-mail: matteo.moretti@grupposandonato.it

M. Laganà · M. Moretti
Gruppo Ospedaliero San Donato Foundation, Corso Di Porta
Vigentina 18, 20122 Milan, Italy
e-mail: matteo.lagana@mail1.grupposandonato.it

Keywords Microfluidics · Reversible bonding ·
Magnetism · Micropowder · Chondrocyte

1 Introduction

In the last few years, the interest in microfluidic devices for analytical chemistry or biotechnology has been dramatically increasing. Indeed, compared to traditional analytical instruments, microfluidic platforms are characterized by lower reagent consumption, reduced analysis time, lower fabrication costs, and highly controlled environments

(Sui et al. 2007). These advantages depend on the overall miniaturization of the fluidic systems that are commonly obtained by bonding a polymeric layer (usually PDMS) containing the microchannel pathway to a second layer working as substrate (glass or polymer).

The process by which the bonding occurs has a prominent role in securing functional micro-sized channel. Despite its apparent simplicity, indirect bonding by means of an adhesive layer has been successfully reported in only few applications due to the challenge of channel clogging (Rötting et al. 2002; Huang et al. 2007; Dang et al. 2005; Becker and Gartner 2000). Taking into account this severe limitation, most of the devices are based on direct bonding methods that mate the substrates without any additional materials added at the interface (Herold and Rasooly 2009). Among direct bonding methods, thermal (Taberham et al. 2008; Hromada et al. 2008; Buch et al. 2004; Arroyo et al. 2007), solvent (Wallow et al. 2007; Unger et al. 2000; Sun et al. 2006; Griebel et al. 2004; Brydson 1999), and surface modification (Johansson et al. 2002; Brown et al. 2006; Abgrall et al. 2006) techniques have been successfully applied. The latter approach, based on plasma treatment, increases surface adhesiveness removing surface contaminants, roughening bonding surfaces, and increasing surface energy by introducing reactive chemical groups. These modifications enable a more intimate contact between the layers that is further stabilized by chemical reactions occurring at the surfaces, thus ultimately resulting in an enhanced mechanical interlocking (Shenton et al. 2001).

Plasma activation is by far the most common technique in microfluidic application due to the high performances in terms of sealing. Nonetheless, its exploitation is limited to few polymers, needs specific plasma equipment and results in an irreversible bonding that could represent in many cases a critical limitation to the current potential of these devices. Indeed, several applications, including complex cell patterning and surface functionalization as well as insertion and removal of macroscopic, solid or non-injectable samples and analysis techniques, not achievable within the microfluidic devices, would benefit from reversible bonding capabilities.

In order to establish alternative approaches that would allow a better integration of the above-mentioned functions in microfluidic devices, many efforts have been directed in the last years to the development of reversible bonding techniques. These studies aim at attaining an adhesion between layers (microfluidic and substrate) sufficient to withstand the designed microfluidic applications, enabling at the same time a simple access to the “experimental field”.

One of the first methods applied to obtain a reversible sealing takes advantage of the van der Waals attraction

forces operating at the PDMS–PDMS and PDMS–glass interfaces. This sealing method, based on the electrochemical interaction occurring between untreated surfaces, is watertight and rapidly occurs at room temperature just by mating the surfaces. The weak adhesion could be reversed by simply peeling off the PDMS and therefore breaking the seal. However, this technique withstands only low pressures in the channels (previous study assessing approximately 35 kPa) (McDonald et al. 2000).

In order to enhance surface interactions, Khademhosseini et al. (2005) introduced a temporary plasma bonding method; in particular, according to their technique, bonding occurs between two PDMS mating surfaces, of which only one is plasma treated. Despite its simplicity, microchannels reversibly sealed with this method frequently leaked at minimal positive pressures corresponding to minimal flow rates forcing the authors to apply negative pressures to drive the flow.

For applications requiring higher pressures (up to 100 kPa), adhesion of PDMS to glass has been obtained by vacuum application through a dedicated channel network located at the PDMS–glass interface all around fluidic channels (Le Berre et al. 2006); however, this method requires a further design step for the suction network and needs a specific system to provide continuous vacuum.

More recently, Rafat et al. (2009) presented a simple and inexpensive method to fabricate fluidic devices using magnets to reversibly bond PDMS and other polymer matrices to glass or gel substrates. In their work, the attraction forces between small magnets and iron slabs were exploited to guarantee polymer–glass adhesion. Nonetheless, due to the presence of magnets and iron slabs, the possible range of applications is restricted to macroscopic fluid-dynamic devices based on very simple geometries.

In this paper, in order to overcome the limitations of previously published works, we describe, characterize and validate a novel technological approach that extends the magnetic reversible bonding approach to microfluidic-sized devices. A new reversible device has been developed embedding a magnetic suspension in the PDMS, thus permitting the exploitation of the method with complex micro-sized geometries. The effective sealing of fluidic devices by means of the new magnetic approach has been characterized focusing on a branched and multi-sized geometry and demonstrating superior performances as compared to previously published reversible techniques. Finally, cell culture experiments on primary chondrocytes have been conducted showing a simple exploitation of the reversible bonding in histological and fluorescent histochemical analysis that are limited in irreversibly bonded devices.

2 Materials and methods

2.1 Design and fabrication techniques

A two-mold fabrication process has been developed to obtain magnetic devices. Specifically, the process included the manufacturing of a top layer, filled with iron powder and PDMS, and a bottom layer, containing microfluidic channels, few hundred micrometers thick. After bonding the two layers, a histology glass slide was interposed between the assembled PDMS device and a magnet, so to function as substrate for the fluidic channels.

The bottom layer contains the microfluidic channels, and it was realized by means of conventional soft-lithography techniques (Xia and Whitesides 1998) from a silicon mold. Figure 1a refers to the profiles of the channels, drawn by means of CAD software. Two resists were used to achieve different feature sizes on the silicon wafers: SU8-50 (MicroChem Corp) for the 75 μm height/100 μm width channels (so as to form a Y-shaped fluidic path) and AZ-4562 (AZ Electronic Materials GmbH) for the two sets of five parallel channels, 25 μm in height and 50 μm in width. PDMS-prepolymer and curing agent (Sylgard 184, Dow Corning) were then mixed in ratio 20:1 (w/w), stirred and degassed under reduced pressure, and finally spun at a

thickness of 500 μm on the silicon mold and partially pre-cured in oven at 70°C for 40 min.

The top layer was realized by replica molding to obtain cavities apt to contain the magnetic suspension. Two alternative technologies were used so as to achieve different depths of the cavities and, in turns, magnetic adhesion forces.

2.1.1 Thick cavity fabrication

In order to fabricate 3-mm thick cavities, a desktop CNC milling machine (MDX40, Roland DG) with an 800 μm in diameter carbide end mill was used to machine out a flat 5-mm thick PMMA substrate to a final depth of 3 mm (all the fabrication steps are reported in Fig. 1). A 10:1 (w/w) mixture of PDMS was poured into the PMMA mold, cured in oven at 70°C for 120 min and finally left at room temperature to cool down for 30 min. The PDMS structure was gently removed from the mold and subsequently (similarly to the multilayer method introduced by Unger et al. (2000) manually aligned under a stereomicroscope to the partially cured bottom layer (with openings downside) so to enclose an empty volume with the top layer cavities. A further curing step followed in oven at 70°C for 120 min. Iron powder with grain size smaller than 212 μm

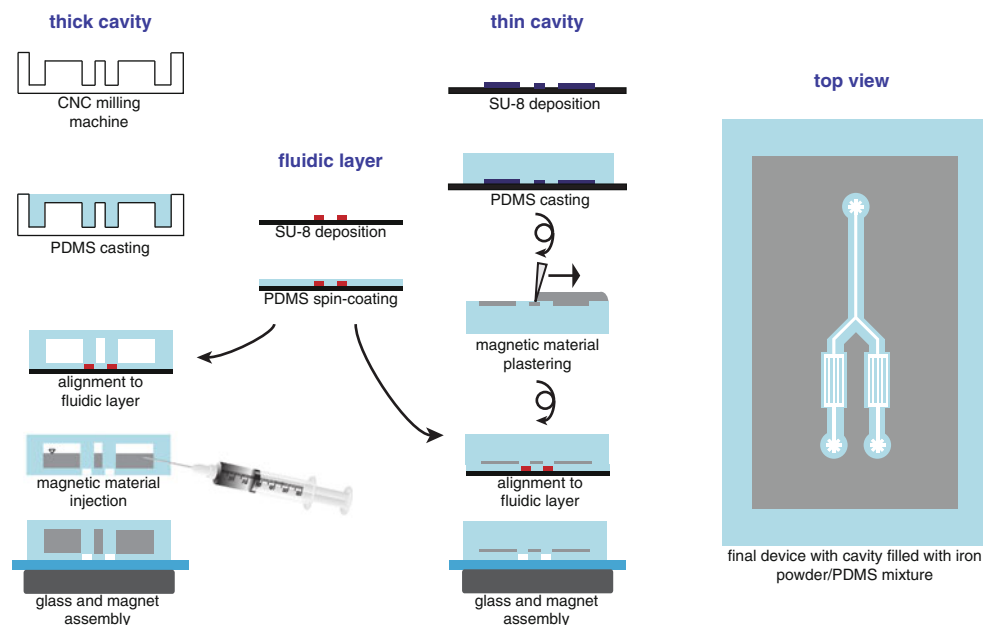


Fig. 1 Fabrication of the magnetic device. To obtain thick cavity devices (“thick cavity” column), a PMMA mold was realized with a CNC milling machine at a final depth of 3 mm; PDMS was cast, aligned, and bonded to the fluidic layer (“fluidic layer column”). Ferromagnetic suspension (iron powder/PDMS mixture at ratio 4:1 as w/w) was then injected in the device’ cavity. Thin cavity device fabrication (“thin cavity” column) only involved soft lithography

techniques. The ferromagnetic suspension was manually plastered into the top layer right before alignment and bonding to the fluidic layer. For both configurations, channels were enclosed with a histology glass slide, and sealing was guaranteed by the presence of a neodymium magnet. The top view of the final assembled devices (identical for both configurations) is also sketched so as to show the channel layout and the cavity outline

(Sigma-Aldrich Corp) was mixed at 4:1 (w/w) with PDMS (base/curing agent ratio 10:1). After degassing, the iron/PDMS mixture was poured in a 2.5-ml plastic syringe and injected in the microfluidic device cavity by means of a needle. A final curing step was performed in oven at 70°C for 120 min.

2.1.2 Thin cavity fabrication

As an alternative, soft lithography was used to produce a silicon/SU8-2150 (MicroChem Corp) mold with the same layout previously described, but different in that the final feature height was set to 500 μm (steps described in detail in Fig. 1). A 10:1 (w/w) mixture of PDMS was poured into the mold, cured in oven at 70°C for 120 min and finally left at room temperature to cool down for 30 min. After removing this latter top layer, iron powder/PDMS mixture at a concentration of 4:1 (w/w) was directly plastered into its cavities; the material in excess was removed with a flat blade prior a curing step in oven at 70°C for 60 min. Manual alignment between the two layers was performed under a microscope taking advantage of the optical transparency of the top layer in the channel regions. A final curing step was performed in oven at 70°C for 120 min.

2.1.3 Final assembly

After punching input and output ports, the fluidic devices were finally assembled closing the channels against a histology glass, and by placing a neodymium magnet (40 \times 20 \times 10 mm, magnetization N42) on the opposite side.

Thanks to this manufacturing technique, direct optical inspection of microfluidic channels is possible through the top layer. The top view of the final assembled device is also shown in Fig. 1, where the cavity borders outline the limit of optical transparency.

2.2 Sealing characterization

In order to evaluate the bonding strength of magnetic forces, sustainable pressure, achievable flow rates, and their mutual hydraulic relation were studied by means of static and dynamic experiments. To this purpose, the magnetic microfluidic devices were bonded to polylysine-coated glass slides by means of a magnet positioned as described in Fig. 1 and continuously maintained in situ throughout the experiments. This configuration was referred to as continuously applied magnet (either CAM or μCAM corresponding to the 3-mm or 500- μm thick cavity devices, respectively). Two alternative configurations were used: (i) temporary applied magnet (TAM and μTAM), in which magnets were removed after 60 min and before the

application of pressure/flow, (ii) no magnet (NoM), obtained by contacting the magnetic devices to the histological slide, without applying any magnet. A reversible bonding technique from literature was adopted as control: reference reversible bonding (RRB) devices were obtained by plasma treating the PDMS layer containing channels (base curing ratio 10:1 (w/w)) and not the corresponding substrate (Khademhosseini et al. 2005).

In one experiment, pure PDMS devices (base/curing ratio 10:1 w/w) were also cast on the silicon mold, and permanently bonded to histology glass slides by means of plasma treatment (30 s), followed by 20 min in oven at 70°C. This configuration was referred as permanent plasma bonding (PPB).

All devices were preconditioned prior to usage by subsequently injecting (10 $\mu\text{l}/\text{min}$, 3 min) with a syringe pump (PHD 22/2000, Harvard Apparatus): (1) ethanol 70% v/v, (2) double distilled water (ddH_2O).

2.2.1 Static sealing

In order to identify the maximal static pressure that each reversible configuration could withstand, a precision pressure regulator (IR2010, SMC Corp) was used. After the preconditioning step, the two inlet ports of the microfluidic device were connected to the regulator through tubes containing color label and the outlet clamped. Pressure slopes were then applied at increasing discrete steps of 5 kPa/min. The maximum pressure value for each configuration was determined at a point where menisci (color label/air interface) in the inputs started moving toward the device, corresponding to a leakage occurrence. For each configuration three devices were tested ($n = 3$).

2.2.2 Dynamic sealing

To assess the maximum flow rates that different devices could withstand, all configurations (except PPB) were tested applying increasing flow rates. After preconditioning, a syringe pump, simultaneously controlling two plastic syringes, was connected to both the input ports of the device and used to inject fluid. Color label was perfused through the channels at increasing flow rates with steps of 10 $\mu\text{l}/\text{min}$ until 400 $\mu\text{l}/\text{min}$ and subsequently steps of 50 $\mu\text{l}/\text{min}$ until 1000 $\mu\text{l}/\text{min}$. Each flow rate was maintained constant for 120 s. Maximum sustainable flow rates were determined at the point where leakages appeared under microscope. For each configuration three devices were tested ($n = 3$).

2.2.3 Aptitude to reusability

Supplementary experiments were performed in order to assess the degradation of the devices after first usage. To

this purpose, five consecutive dynamic leakage tests were conducted on all configurations except PPB (three devices for each configuration, $n = 3$). After each test, the devices were rinsed first with distilled water, then with ethanol and finally air dried, before being tested again.

2.2.4 Hydraulic characterization

In order to obtain flow-pressure curves, a dynamic setup was chosen, different from the dynamic leakage configuration in that the pressure was the controlled value. Aim of this experimental setup was to evaluate possible modifications to the hydraulic resistance of CAM devices due to the pressure exerted by the magnet. A precision pressure regulator was used to accurately apply pressure to a closed reservoir containing color label. After conditioning steps, the reservoir was connected to one of the two input ports of the fluidic device by means of polyethylene tubing, while the other input port was clamped. The applied pressure was linearly increased from 10 to 50 kPa, in steps of 10 kPa, and kept constant for 120 s at each value. Flow rates were determined by measuring the weight of the accumulated liquid volume, collected from the outlet port. PPB devices were used as control, and five devices were tested for each configuration ($n = 5$).

2.2.5 Effects of the iron powder content

To evaluate the effects of iron powder content in the ferromagnetic suspension, different configurations were realized, by varying both cavity thickness (0.5, 1, 2, and 3 mm) and iron powder concentration in the mixture (1:1, 2:1, 3:1, and 4:1 as w/w). Combinations of such parameters, yielded to 16 configurations, tested in three replicates in terms of maximum sustainable pressure.

2.2.6 Statistical analysis

Statistical analyses were carried out by one-way ANOVA and all pairwise multiple comparisons were carried out using the Holm-Sidak method with $P < 0.05$ considered significant.

2.3 Cell experiments

2.3.1 Cell isolation and expansion

Adult human articular cartilage samples were aseptically harvested from discarded knee fragments obtained during routine arthroplasty surgical procedures, with the patient's informed consent. Chondrocytes were isolated by digestion in 0.15% type II collagenase (Worthington) for 22 h at 37°C, 5% CO₂ (Démarteau et al. 2003), and plated for

expansion at 10⁴ cells/cm² in basic medium (Dulbecco's Modified Eagle Medium containing 10% fetal bovine serum (Lonza), 1 mM sodium pyruvate, 100 mM HEPES buffer, 100 U/ml penicillin, 100 µg/ml streptomycin, 0.29 mg/ml L-glutamine) supplemented with 1 ng/ml TGF-β1, 5 ng/ml FGF-2 (both from PreproTech), hereby called complete medium (CM) (Jakob et al. 2001). After approximately 10 days, when cells were sub-confluent, cells were detached using 0.15% type II collagenase (10 min) and 0.25% trypsin/1 mM EDTA (5 min) and resuspended in CM at 2 × 10⁷ cells/ml for seeding. If not otherwise specified, Invitrogen products were used.

2.3.2 Cell seeding

CAM devices were preconditioned before cell seeding with subsequent injections (10 µl/min, 3 min) of: (1) ethanol 70% v/v, (2) phosphate buffer solution (PBS), (3) CM, and stored overnight at 37°C, 5% CO₂ filled with CM. The cells were then seeded in the device through the double channel side at a flow rate of 2.5 µl/min. After a subsequent flow reversion (10 s at 2.5 µl/min), the syringe pump was stopped and all the connection tubes were clamped. After seeding, devices were incubated for 4 h at 37°C, 5% CO₂ for cell adhesion (clamps were removed after 1 h).

2.3.3 Histology and histochemistry

After 4 h, the magnets were removed from the devices and phase contrast images of the channels with seeded cells were acquired at the microscope. Forthwith, the PDMS structure was removed from the glass slide in order to perform the histological and histochemical analyses of adherent cells. Exposed glass slides were transferred in Petri dishes and rinsed twice in PBS. After removing the PBS, formaldehyde 4% was added to fix the samples (10 min at room temperature) followed by two PBS rinsing steps. Fixed samples were either immediately used for subsequent analysis or stored in PBS at 4°C. For hematoxylin/eosin staining, previously published protocols were adopted (Fischer et al. 2008). The samples were stained by F-actin BODIPY[®]FL phalloidin (Invitrogen) and nuclei counterstained with DAPI (Invitrogen) according to manufacturer protocols. All phase contrast, bright field, and fluorescent images were acquired using an IX71 inverted microscope (Olympus Corp).

3 Results

Pictures of the thick magnetic devices realized are shown in Fig. 2. The developed devices were made by permanently bonding two PDMS layers: (i) a top layer hosting

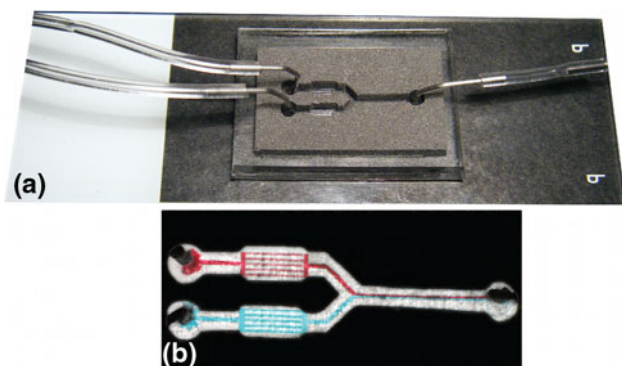


Fig. 2 Leak-proof reversibly bonded microfluidic device. In **a** an image of the reversibly bonded device on a histology glass slide. In **b** an image of two parallel color labels generated in the microfluidic channels at a flow rate of 400 $\mu\text{l}/\text{min}$. The flow was confined within the microchannel along the entire fluidic pathway proving the effective sealing of the magnetic device

cavities filled with PDMS/iron powder suspension, and (ii) a bottom layer containing fluidic channels. The microfluidic pathway was chosen in order to be representative of devices presenting multiple branches and channels with different sizes; two sets of smaller channels were designed to test the adhesion of the device in multi-branched regions where, due to the high channel density, no iron powder was present. A thin glass slide (histology glass) interposed between the assembled devices and a permanent magnet ensures the water tightness of the microchannels in a reversible way. Thanks to its design specifications, the device allows optical inspection: (i) while a magnet is applied using a stereomicroscope and a point light source; (ii) after magnet removal, using a transmitted light phase contrast microscope. The picture in Fig. 2b, taken after magnet removal, shows the confined flow of the two color labels (red and blue) in both the 100 and 50 μm channels, with the classical non-mixing laminar flow configuration within the single microchannel.

3.1 Sealing results

3.1.1 Static sealing

In order to evaluate the bonding strength of magnetic forces, maximum sustainable static pressure was measured for CAM, μCAM , TAM, μTAM , NoM and RRB configurations. Summarizing the average pressure values that each configuration could withstand, Fig. 3 shows that magnetic devices had a better performance in terms of maximum sustainable pressure (58.3 ± 2.9 and 26.7 ± 2.9 kPa for CAM and μCAM , respectively) than the other configurations. NoM devices, relying only on van der Waals adhesion of PDMS to glass withstood a pressure of 18.3 ± 5.8 kPa, while the weakest sealing ability was noticed for

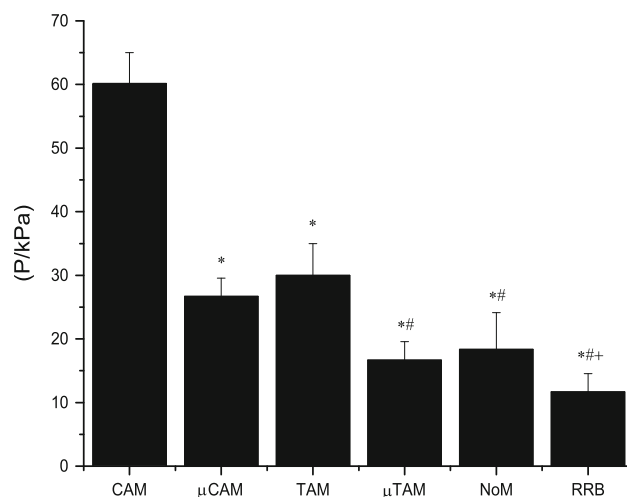


Fig. 3 Results of the static leakage experiments. A precision pressure regulator was used to provide steps of 5 kPa to the device input ports, while their output ports were clamped. The maximum pressure value for each configuration was determined at a point where menisci (color label/air interface) in the input tubes started moving toward the input ports of the devices (corresponding to a leakage occurrence). For each configuration, a set of three experiments was performed with three devices. Mean values \pm SD. * $P < 0.05$ compared with CAM. # $P < 0.05$ compared with μCAM and TAM. + $P < 0.05$ compared with μTAM and NoM

RRB devices (11.7 ± 2.9 kPa). In addition, the temporary application of the magnet seemed to bring a benefit in terms of adhesion strength only for higher ferromagnetic volumes. TAM devices, in fact, showed a significantly higher sealing ability than NoM and RRB devices (and comparable with μCAM), while μTAM was not significantly different from NoM.

3.1.2 Dynamic sealing

With the purpose of investigating the dynamic leakage, increasing flow rates were applied until device failure occurrence. The maximum flow rates that the different configurations could withstand are shown in Fig. 4.

As for the μTAM , NoM, and RRB devices, consistent leakages were observed above 383 ± 28 , 367 ± 29 and 63 ± 20 $\mu\text{l}/\text{min}$, respectively. The liquid outflow randomly occurred with no specific regions being more subjected to leakage than others. CAM, TAM, and μCAM devices were able to sustain significantly higher flow rates. Indeed, leakages were observed at flow rates as high as 967 ± 58 , 667 ± 58 , and 583 ± 28 $\mu\text{l}/\text{min}$, respectively. Moreover, CAM, μCAM , and TAM devices showed a behavior not evidenced by the other configurations. At flow rates higher than 500 $\mu\text{l}/\text{min}$, a small leakage of fluid was observed, confined within the five smaller channels regions, thus creating a hydraulic connection amongst parallel confining channels. This observed “confined leakage” had two

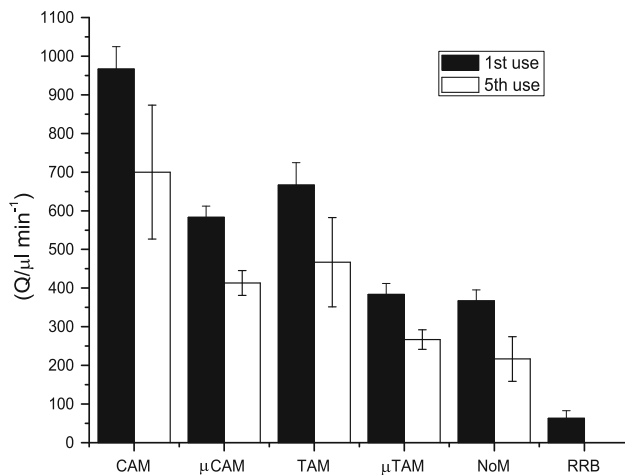


Fig. 4 Results of the dynamic leakage experiments in terms of maximum allowed flow rates. A syringe pump was used to simultaneously control two 20 ml syringes, thus perfusing the devices at controlled flow rates. Leakage occurrences were inferred by optical observation under microscope, and the corresponding flow rates value were recorded. The first column shows the maximum sustainable flow rates at the first dynamic sealing experiment. The second column shows the maximum sustainable flow rates after six dynamic sealing experiments. For RRB configuration, the sustainable flow rate at fifth usage is not reported since at the third usage a sealing failure occurred. For each configuration, a set of three experiments was performed. All the data are shown as mean values \pm SD

characteristics: (i) stability, as it was confined within the smaller channels region, even at higher flow rates; (ii) reversibility, as by simply decreasing the flow rate applied, the fluid flow resulted again confined within original channels.

3.1.3 Aptitude to reusability

In order to study the degradation of the sealing performances over repeated usage, single devices were tested up to five times. The results (also reported in Fig. 4) show that all the configurations underwent a progressive degradation with percentages of flow rate loss ranging from 24 to 31%. NoM was able to withstand a final maximum flow rate equal to $217 \pm 58 \mu\text{l/min}$. CAM and μCAM presented greater percentage losses with final maximum flow rates equal to 700 ± 173 , and $413 \pm 32 \mu\text{l/min}$, respectively. TAM and μTAM had a similar loss, with final values of 467 ± 29 , and $267 \pm 25 \mu\text{l/min}$, respectively. RRB devices did not seal at all after third usage, the latter corresponding to a maximum sustainable flow rate of $25 \mu\text{l/min}$.

3.1.4 Hydraulic characterization

With the aim of studying the possible deformations of channels due to magnetic bonding technique (based on compressive forces rather than adhesive forces), CAM and

PPB devices were evaluated applying known inlet pressures and measuring the flow rates at the outlet. The results, shown in Fig. 5, demonstrate that at low pressure values (10–20 kPa) CAM devices had higher hydraulic resistances, as demonstrated by lower measured flow rates, as compared to PPB devices. At 30 kPa, the two configurations provided similar flow rates ($285 \pm 5 \mu\text{l/min}$ for CAM and $296 \pm 14 \mu\text{l/min}$ for PPB), demonstrating therefore similar hydraulic resistance. By further increasing the external pressure, the flow rates measured within CAM devices overcome those in the PPB, this most likely depending on a lower hydraulic resistance of the device.

3.1.5 Effects of the iron powder content

The influence of the ferromagnetic content on the magnetic strength was assessed through static leakage tests. Figure 6 shows how the increase of the iron powder/PDMS mixture volume (reported as cavity thickness) also corresponds to an increase in terms of sealing ability. Similar behavior was observed by varying the iron concentration in the mixture. At low ferromagnetic grades and/or cavity thicknesses, the devices behaved as NoM, meaning that the influence of magnetism was negligible with the respect to van der Waals forces. For this purpose, Fig. 6 also shows

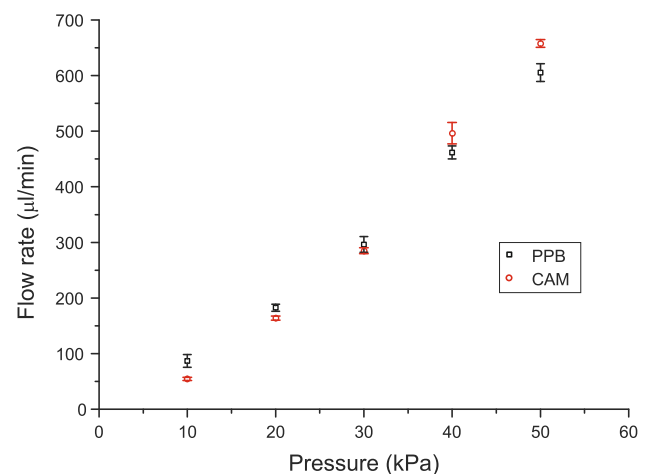


Fig. 5 Results of the hydraulic characterization experiments of the magnetic devices. At small pressures smaller flow rates were recorded as compared to undeformed devices (PPB), thus suggesting that magnetic forces pressed the device upper walls toward the histology glass slides. For higher pressures (around 30 kPa) the magnetic forces balanced the hydrostatic pressure force acting within the channels, and the cross-sectional areas of CAM and PPB devices were similar. By further increasing the applied pressure, the regions where no magnetic material was present started detaching from the glass substrate, increasing the cross-sectional area (which in turns decreased the hydraulic resistance). This behavioral change happened at an applied pressure value of 40 kPa. It is important to notice that the flow rate at which the hydraulic resistance drop occurred correspond to a value of about $500 \mu\text{l/min}$. All the data are shown as mean values \pm SD

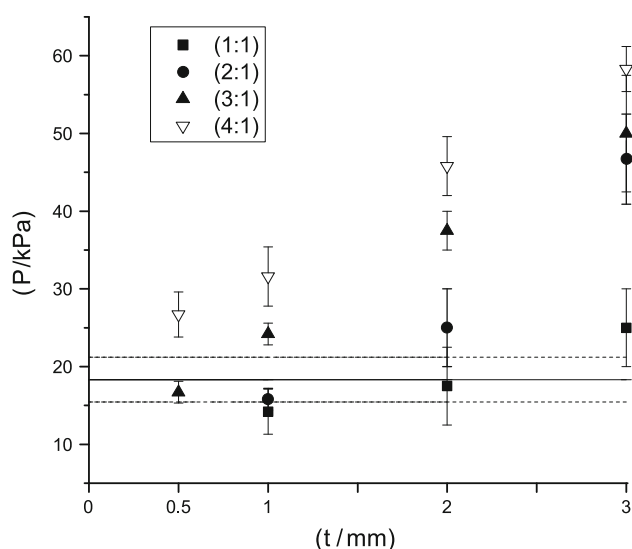


Fig. 6 Effects of the iron powder content on the sustainable pressure. In general, at increasing magnetic suspension thickness (t), the pressure each device can withstand also increases. Four concentrations of iron powder in the ferromagnetic suspension were tested for each thickness, with the exception of the 500 μm device (concentrations below 4:1 in w/w were not significantly different). The horizontal continuous line represents the average value for NoM device ($\pm\text{SD}$ as *dashed lines*). Data points above this line indicate that magnetic bonding is advantageous with the respect to simple van der Waals interactions

the NoM results as a band region (mean \pm SD), above which the use of magnetic devices is beneficial.

3.2 Cell experiments

To finally assess the exploitation of reversible sealing in cell culture experiments, primary chondrocytes were seeded in magnetic devices. After 4 h incubation the magnet was removed (without leakage occurring) and phase contrast images of the device were taken. The micrograph (Fig. 7a) shows homogeneously seeded microfluidic devices. The cells spread on the polylysine coated glass slides resulting in a semi-confluent monolayer covering microfluidic channels. A negligible number of non-adherent cells were present in the channels along with an adherent population that did not display any sign of sufferance or apoptosis as far as cell morphology was concerned (Fig. 7c).

Taking advantage of the reversible bonding, the microfluidic device was carefully disassembled and the exposed cell monolayer fixed. The direct access to the cultured cells allowed to stain the monolayer for hematoxylin and eosin (Fig. 7b), following a traditional protocol not suitable for PDMS microfluidic devices being one of the chemicals, namely xylene, a solvent of PDMS.

4 Discussion

In this work, we presented a reliable method to fabricate reversibly bonded devices with micrometer-sized channels and branched fluidic configurations. The interest in realizing devices able to be disassembled is recently growing, and a number of techniques have been proposed (Rafat et al. 2009; Le Berre et al. 2006; Khademhosseini et al. 2005). In general, reversible sealing occurs because PDMS is flexible and can conform to minor imperfections in a flat surface making intimate contact with it. Based on this property, reversibility has so far mainly relied on two distinct effects: van der Waals forces (NoM) (Pocius 2002) and partial plasma treatment (RRB) (Khademhosseini et al. 2005). However, no satisfying results in terms of maximum sustainable pressures have been obtained, thus limiting the range of its applicability. More recently, new approaches have been proposed to overcome such a limitation. In particular, Rafat et al. (2009) presented a PDMS-based fluidic device able to guarantee hydraulic tightness by embedding magnet slabs in the material bulk, and placing an iron bar underneath. The use of a magnetic field is promising in that adhesion forces generated by a permanent magnet do not require any additional power source, and allow keeping overall dimensions relatively small. However, in their work, Rafat et al. (2009) only dealt with millimeter-sized straight channels. Due to the use of iron slabs their method was then not directly applicable to micrometer-sized complex fluidic geometries, and a further step in the fabrication technique was necessary.

The method here proposed was tested on a Y-shaped geometry including smaller parallel channels in each branch so as to be generally representative of complex geometries. The device fabrication relied on a two-step process: a standard PDMS casting from a silicon wafer mold obtained through soft-lithography (for channel layer fabrication), and a PDMS replica molding, for magnetic suspension confinement. As a consequence of the specific fabrication process, the regions enclosing microfluidic channels were optically transparent so that standard laboratory microscopy techniques could be applied to monitor the experiments.

To properly study and compare the bonding characteristics and the sealing performances of our magnetic approach, the same fluidic layout was replicated and tested in different configurations (NoM, RRB, CAM, μCAM , TAM, and μTAM). This was done because literature-derived values could not be used as reliable terms of comparison since parameters such as flow rates and pressures are strongly dependant on employed geometries and materials.

Both static and dynamic experiments demonstrated the ability of the magnetic devices to withstand higher

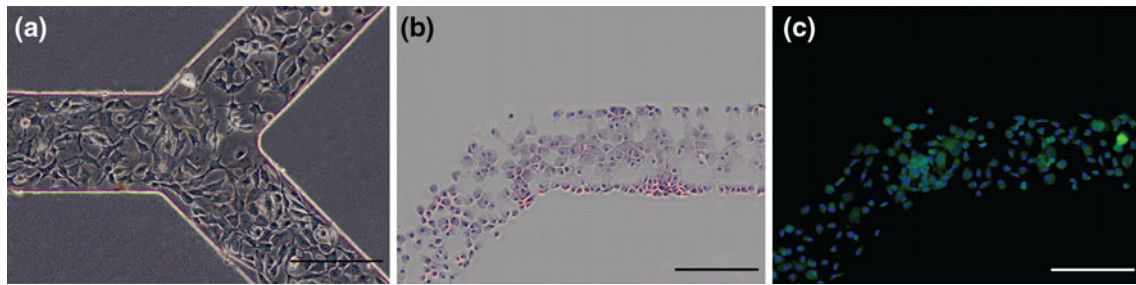


Fig. 7 Reversible devices seeded with primary chondrocytes. Cell adhesion was evaluated 4 h after seeding by phase contrast imaging through to the transparent PDMS layer overlaying the channels (a). Cells, confined within the channels, were homogeneously distributed through the device resulting in a semi-confluent mono layer of spread cells with no evident signs of cell sufferance. After removing the polymeric layer of the microfluidic devices the exposed cell

monolayer was fixed and the resulting glass slides used for further analyses. Samples were either stained with hematoxylin eosin according standard histological protocol (b) or histochemically stained by F-actin (BODiPY®FL phalloacidin) with a nucleic counterstaining (DAPI) (c). Both the images show negligible cell layer damage upon disassembling as compared to phase contrast image. Scale bars are 200 μm

pressures and flow rates than other configurations; in particular CAM devices were able to reach pressures about three and five times higher than those obtained by NoM and RRB, respectively. Surprisingly, reported results show that the magnet has a significant effect in increasing the sealing performances not only if continuously applied (CAM and μCAM) but also when used to create a more intimate surface contact for a given time and finally removed before pressure application (TAM). By only relying on data presented in literature (McDonald et al. 2000; Sui et al. 2007), NoM devices would be expected to withstand inner pressures as high as 35 kPa. However, as shown with our configuration, NoM devices were only able to achieve a maximum pressure of about 18 kPa before leakage. As previously stated, differences can be related to channel design geometry. We hence suggest significant care should be taken when comparing data derived from literature by evaluating the conditions and moreover geometries and materials of the specific microfluidic devices.

In addition, dynamic experiments evidenced another relevant phenomenon occurring within the parallel channels sites for CAM, μCAM , and TAM devices. At flow rates below 500 $\mu\text{l}/\text{min}$, the fluid was able to flow without leakages along the channels, while above this value a “confined leakage” effect was noticed in the small multi-branched channel regions. Interestingly, this “confined leakage” showed a distinctive reversible feature, i.e. when the flow rate was reduced, fluid flow was reversibly confined within the channels. Although further studies are needed in order to better characterize this phenomenon, we suggest that a possible application of the confined leakage could be the realization of pressure-dependent fluidic valves allowing temporary communication through walls among adjacent channels.

The influence of the ferromagnetic material content within the devices was also investigated, showing an

increase of their ability to withstand pressure together with the iron powder grade and volume. Iron powder/PDMS suspensions at concentrations above 4:1 (w/w) were not tested due to the difficulty of a manual uniform mixing, although higher iron contents could be easily achieved through mechanical processing.

A hydraulic characterization of CAM and PPB devices was performed in order to evaluate possible effects induced by the magnetic forces on the device hydraulic resistance, as a result of induced deformations to the channel geometry. At low pressures, smaller flow rates were recorded as compared to undeformed devices (PPB), thus suggesting that magnetic forces pressed the device upper walls toward the histology glass slides. For higher pressures (around 30 kPa), the magnetic forces balanced the hydrostatic pressure force acting within the channels, giving rise to similar hydrodynamic characteristics for CAM and PPB devices. By further increasing the applied pressure, the regions where no magnetic material was present (each of the parallel channels set) started detaching from the glass substrate, increasing the cross-sectional area (which in turns decreased the hydraulic resistance). This behavioral change happened at an applied pressure value of 40 kPa. It is important to notice that the flow rate at which the hydraulic resistance drop occurred correspond to a value of about 500 $\mu\text{l}/\text{min}$, which is also the threshold value at which the “confined leakage” effect was observed during dynamic experiments.

Removal of the microfluidic PDMS layer results in a direct accessibility to the samples. As compared to permanently bonded systems, advantages can derive from the possibility to analyze samples by means of assays that cannot be applied either in presence of PDMS or other polymers (e.g. for incompatible chemicals or temperatures), or in microchannels where the perfusion of each solution is limited by maximal allowed flow rates to prevent cell detachment. Biologically relevant examples are

the biochemical and histological assays that often rely on several incubation and rinsing steps with tight timing constraints, which cannot always be easily transferred in a microfluidic environment (perfusion timing shift and/or cell loss due to shear stress). In this work, magnetic microfluidic devices were used as cell culture platforms for human chondrocytes. To demonstrate an example of direct advantage of the reversible bonding technique, cells were stained to highlight actin and nuclei using a standard histochemical protocol characterized by incubation and several rinsing steps. These steps were performed on the same histology glass slide used for cell culture upon PDMS layer removal. During experiments, device disassembling showed no significant cell losses, as evidenced by monolayers stained by hematoxylin and eosin and for F-actin.

In the presented setup, the highest performances in terms of sustainable pressure and flow rate were observed in micro-machined devices, for which the maximum achievable complexity of the channels fluidic network was only limited by the lateral resolution provided by the employed CNC milling machine (800 μm). To provide more flexible and accurate solutions for even more complex channel designs, an alternative fabrication process was described and characterized, which only involved soft-lithography techniques. The low ferromagnetic suspension thickness achievable with this method also reduces the overall hydraulic performances. For this reason, we suggest that a multiple step soft-lithography process should be used whenever high lateral resolutions are needed.

The presented method offers new perspectives to microfluidic applications. So far microfluidic bioreactors have been limited to seed and grow three-dimensional (3D) cell cultures (Fischer et al. 2008), either for drug screening (Pocius 2002) or 3D construct generation (Ong et al. 2008). On the contrary, our method allows for insertion and removal of solid 3D constructs during experiments, thus possibly being an enabling tool for their transfer into a larger scale. A further application is the on-chip protein crystallization, where the postcrystallization extraction from microfluidic devices is still a delicate step, and source of possible damages for crystals and for membrane proteins, due to their high solvent content (Li and Ismagilov 2010).

In addition, our method allows to generate flow rates two and a half times higher than previously reported methods (Sui et al. 2007), and up to 2.2 in Reynolds number. Thus, applications requiring high flow rates could be explored, and take advantage of a reliable reversible bonding approach. Recently, a microfluidic device for blood plasma separation was successfully introduced, achieving satisfactory performances only at flow rates higher than 200 $\mu\text{l}/\text{min}$ (Rodriguez-Villarreal et al. 2010). Moreover, mixing at the microscale still remains an open

problem, whereby high throughput chemical micro-reactors can take advantage from high flow rate regimes (Jang et al. 2008), thus consistently reducing the time scale of the single fluidic step.

Compared to plasma treatment, this type of bonding procedure can potentially be applied to a series of materials that are poorly exploited in microfluidics. Relevant examples could be hydrogels and other flexible polymers, which can offer new cell material interaction perspective as well as better chemical compatibility. The increased number of steps necessary to generate the single device could be justified by the experimental results demonstrating that magnetic devices would be re-used several times without a significant loss in terms of sealing ability.

5 Conclusions

We implemented and characterized a novel method that allows to reversibly assemble microfluidic devices. A wide range of hydrodynamic conditions was tested. The magnetic devices fabricated have shown significantly higher performances than other devices obtained with classical approaches for reversible bonding. Moreover, the encouraging results offered by TAM devices suggest that the use of the magnet could be limited to the most critical experimental steps (whenever high flow rates/pressure applied are needed), while it could be removed during observation under microscope, so as to profit from the device full optical transparency.

Acknowledgments The authors appreciate helpful conversations with Dr Giancarlo Franceschetti, who made important contributions to the formative stages of this research. The authors also thank Mara Licini, Clara Nozza, Alice Sormani and Lia Volpatti for their valuable help during hydraulic measurements. This work was partially supported by Cariplo Foundation grant # 2008-2531 and Progetto Roberto Rocca.

References

- Abgrall P, Lattes C, Conédéra V, Dollat X, Colin S, Gué AM (2006) A novel fabrication method of flexible and monolithic 3d microfluidic structures using lamination of. *J Micromech Microeng* 16(1):113–121
- Arroyo MT, Fernández LJ, Agirregabiria M, Ibañez N, Aurrekoetxea J, Blanco FJ (2007) Novel all-polymer microfluidic devices monolithically integrated within metallic electrodes for sds-cge of proteins. *J Micromech Microeng* 17(7):1289–1298
- Becker H, Gartner C (2000) Polymer microfabrication methods for microfluidic analytical applications. *Electrophoresis* 21(1): 12–26. doi:10.1002/(SICI)1522-2683(20000101)21:1<12:AID-ELPS12>3.0.CO;2-7
- Brown L, Koerner T, Horton JH, Oleschuk RD (2006) Fabrication and characterization of poly(methylmethacrylate) microfluidic

- devices bonded using surface modifications and solvents. *Lab Chip* 6(1):66–73. doi:[10.1039/b512179e](https://doi.org/10.1039/b512179e)
- Brydson J (1999) *Plastics materials*, 7th edn. Elsevier, Amsterdam
- Buch JS, Kimball C, Rosenberger F, Highsmith WE Jr, DeVoe DL, Lee CS (2004) DNA mutation detection in a polymer microfluidic network using temperature gradient gel electrophoresis. *Anal Chem* 76(4):874–881. doi:[10.1021/ac034913y](https://doi.org/10.1021/ac034913y)
- Dang F, Shinohara S, Tabata O, Yamaoka Y, Kurokawa M, Shinohara Y, Ishikawa M, Baba Y (2005) Replica multichannel polymer chips with a network of sacrificial channels sealed by adhesive printing method. *Lab Chip* 5(4):472–478. doi:[10.1039/b417398h](https://doi.org/10.1039/b417398h)
- Démarteau O, Wendt D, Braccini A, Jakob M, Schafer D, Heberer M, Martin I (2003) Dynamic compression of cartilage constructs engineered from expanded human articular chondrocytes. *Biochem Biophys Res Commun* 310(2):580–588. doi:[S0006291X03018655](https://doi.org/S0006291X03018655)
- Fischer AH, Jacobson KA, Rose J, Zeller R (2008) Media for mounting fixed cells on microscope slides. *Cold Spring Harb Protoc* 4. doi:[10.1101/pdb.ip52](https://doi.org/10.1101/pdb.ip52)
- Griebel A, Rund S, Schonfeld F, Dorner W, Konrad R, Hardt S (2004) Integrated polymer chip for two-dimensional capillary gel electrophoresis. *Lab Chip* 4(1):18–23. doi:[10.1039/b311032j](https://doi.org/10.1039/b311032j)
- Herold KE, Rasooly A (2009) *Lab-on-a-chip technology, vol 1: fabrication and microfluidics*. Caister Academic Press, Norfolk
- Hromada LP, Nablo BJ, Kasianowicz JJ, Gaitan MA, DeVoe DL (2008) Single molecule measurements within individual membrane-bound ion channels using a polymer-based bilayer lipid membrane chip. *Lab Chip* 8(4):602–608. doi:[10.1039/b716388f](https://doi.org/10.1039/b716388f)
- Huang FC, Chen YF, Lee GB (2007) Ce chips fabricated by injection molding and polyethylene/thermoplastic elastomer film packaging methods. *Electrophoresis* 28(7):1130–1137. doi:[10.1002/elps.200600351](https://doi.org/10.1002/elps.200600351)
- Jakob M, Demarteau O, Schafer D, Hintermann B, Dick W, Heberer M, Martin I (2001) Specific growth factors during the expansion and redifferentiation of adult human articular chondrocytes enhance chondrogenesis and cartilaginous tissue formation in vitro. *J Cell Biochem* 81(2):368–377. doi:[10.1002/1097-4644\(20010501\)81:2<368:AID-JCB1051>3.0.CO;2-J](https://doi.org/10.1002/1097-4644(20010501)81:2<368:AID-JCB1051>3.0.CO;2-J)
- Jang K, Sato K, Igawa K, Chung U-i, Kitamori T (2008) Development of an osteoblast-based 3d continuous-perfusion microfluidic system for drug screening. *Anal Bioanal Chem* 390(3):825–832. doi:[10.1007/s00216-007-1752-7](https://doi.org/10.1007/s00216-007-1752-7)
- Johansson BL, Larsson A, Ocklund A, Öhrlund Å (2002) Characterization of air plasma-treated polymer surfaces by ESCA and contact angle measurements for optimization of surface stability and cell growth. *J Appl Polym Sci* 86(10):2618–2625. doi:[10.1002/app.11209](https://doi.org/10.1002/app.11209)
- Khademhosseini A, Yeh J, Eng G, Karp J, Kaji H, Borenstein J, Farokhzad OC, Langer R (2005) Cell docking inside microwells within reversibly sealed microfluidic channels for fabricating multiphenotype cell arrays. *Lab Chip* 5(12):1380–1386. doi:[10.1039/b508096g](https://doi.org/10.1039/b508096g)
- Le Berre M, Crozatier C, Velve Casquillas G, Chen Y (2006) Reversible assembling of microfluidic devices by aspiration. *Microelectron Eng* 83(4–9):1284–1287. doi:[10.1016/j.mee.2006.01.257](https://doi.org/10.1016/j.mee.2006.01.257)
- Li L, Ismagilov RF (2010) Protein crystallization using microfluidic technologies based on valves, droplets, and slipchip. *Annu Rev Biophys* 39(1):139–158. doi:[10.1146/annurev.biophys.050708.133630](https://doi.org/10.1146/annurev.biophys.050708.133630)
- McDonald JC, Duffy DC, Anderson JR, Chiu DT, Wu H, Schueller OJ, Whitesides GM (2000) Fabrication of microfluidic systems in poly(dimethylsiloxane). *Electrophoresis* 21(1):27–40. doi:[10.1002/\(SICI\)1522-2683\(2000101\)21:1<27:AID-ELPS27>3.0.CO;2-C](https://doi.org/10.1002/(SICI)1522-2683(2000101)21:1<27:AID-ELPS27>3.0.CO;2-C)
- Ong SM, Zhang C, Toh YC, Kim SH, Foo HL, Tan CH, van Noort D, Park S, Yu H (2008) A gel-free 3d microfluidic cell culture system. *Biomaterials* 29(22):3237–3244. doi:[10.1016/j.biomaterials.2008.04.022](https://doi.org/10.1016/j.biomaterials.2008.04.022)
- Pocius A (2002) *Adhesion and adhesives technology: an introduction*, 2nd edn. Hanser/Gardner Publications, Cincinnati
- Rafat M, Raad DR, Rowat AC, Auguste DT (2009) Fabrication of reversibly adhesive fluidic devices using magnetism. *Lab Chip* 9(20):3016–3019. doi:[10.1039/b907957b](https://doi.org/10.1039/b907957b)
- Rodriguez-Villarreal AI, Arundell M, Carmona M, Samitier J (2010) High flow rate microfluidic device for blood plasma separation using a range of temperatures. *Lab Chip* 10(2):211–219. doi:[10.1039/b904531g](https://doi.org/10.1039/b904531g)
- Rötting O, Röpke W, Becker H, Gärtner C (2002) Polymer microfabrication technologies. *Microsyst Technol* 8(1):32–36. doi:[10.1007/s00542-002-0106-9](https://doi.org/10.1007/s00542-002-0106-9)
- Shenton MJ et al (2001) Adhesion enhancement of polymer surfaces by atmospheric plasma treatment. *J Phys D* 34(18):2754–2760
- Sui G, Lee CC, Kamei K, Li HJ, Wang JY, Wang J, Herschman HR, Tseng HR (2007) A microfluidic platform for sequential ligand labeling and cell binding analysis. *Biomed Microdev* 9(3):301–305
- Sun Y, Kwok YC, Nguyen N-T (2006) Low-pressure, high-temperature thermal bonding of polymeric microfluidic devices and their applications for electrophoretic separation. *J Micromech Microeng* 16(8):1681–1688
- Taberham A, Kraft M, Mowlem M, Morgan H (2008) The fabrication of lab-on-chip devices from fluoropolymers. *J Micromech Microeng* 18(6):064011
- Unger MA, Chou HP, Thorsen T, Scherer A, Quake SR (2000) Monolithic microfabricated valves and pumps by multilayer soft lithography. *Science* 288(5463):113–116. doi:[10.1126/science.288.5463.113](https://doi.org/10.1126/science.288.5463.113)
- Wallow TI, Morales AM, Simmons BA, Hunter MC, Krafcik KL, Domeier LA, Sickafoose SM, Patel KD, Gardea A (2007) Low-distortion, high-strength bonding of thermoplastic microfluidic devices employing case-ii diffusion-mediated permeant activation. *Lab Chip* 7(12):1825–1831. doi:[10.1039/b710175a](https://doi.org/10.1039/b710175a)
- Xia Y, Whitesides GM (1998) Soft lithography. *Annu Rev Mat Sci* 28:153–184. doi:[10.1146/annurev.matsci.28.1.153](https://doi.org/10.1146/annurev.matsci.28.1.153)